Mapping the Allosteric Communication Network of Aminodeoxychorismate Synthase

Florian Semmelmann, Kristina Straub, Julian Nazet, Chitra Rajendran, Rainer Merkl and Reinhard Sterner

Institute of Biophysics and Physical Biochemistry, *University of Regensburg, D-93040 Regensburg, Germany*

Correspondence to Reinhard Sterner: *Reinhard.Sterner@ur.de*
https://doi.org/10.1016/j.jmb.2019.05.021

Abstract

Allosteric communication between different subunits in metabolic enzyme complexes is of utmost physiological importance but only understood for few systems. We analyzed the structural basis of allostery in aminodeoxychorismate synthase (ADCS), which is a member of the family of glutamine amidotransferases and catalyzes the committed step of the folate biosynthetic pathway. ADCS consists of the synthase subunit PabB and the glutaminase subunit PabA, which is allosterically stimulated by the presence of the PabB substrate chorismate. We first solved the crystal structure of a PabA subunit at 1.9-Å resolution. Based on this structure and the known structure of PabB, we computed an atomic model for the ADCS complex. We then used alanine scanning to test the functional role of 59 conserved residues located between the active sites of PabB and PabA. Steady-state kinetic characterization revealed four branches of a conserved network of mainly charged residues that propagate the signal from chorismate at the PabB active site to the PabA active site. The branches eventually lead to activity-inducing transformations at (i) the oxyanion hole motif, (ii) the catalytic Cys-His-Glu triad, and (iii) glutamine binding residues at the PabA active site. We compare our findings with previously postulated activation mechanisms of different glutamine amidotransferases and propose a unifying regulation mechanism for this ubiquitous family of enzymes.

Introduction

Allostery is an integral property of enzymes that allows for the regulation of activity in response to the physiological needs of a cell [1]. Thereby, ligand binding to an *allosteric site* induces signal propagation via protein backbone or amino acid side-chain movements to affect function at a distant *active site*. Understanding the molecular details of signal propagation between the two sites is an important biochemical challenge both for applied and basic protein biochemistry. In applied research, molecular details of allosteric communication have the potential to reveal binding sites for novel drugs that perturb signal propagation [2–8]. In basic research, the identification of signal propagation pathways is crucial for unraveling universal patterns of the underlying dynamic adaptability of enzymes [9].

A paradigm for studying the molecular basis of allosteric communication are glutamine amidotransferases (GATases). GATases form a large enzyme family, whose members are responsible for the incorporation of nitrogen within numerous metabolic pathways [10–12]. Most GATases are bi-enzyme complexes, consisting of a synthase and a glutaminase subunit, whose activities are mutually coupled: Substrate binding to the synthase subunit allosterically induces glutamine hydrolysis to glutamate and ammonia at the glutaminase subunit. Nascent ammonia is then transported through an intermolecular channel to the active site of the synthase subunit, where it reacts with the "waiting" substrate to specific reaction products [13]. While the synthase subunits of the various GATases are structurally diverse, the glutaminases can be categorized into two classes according to their fold and active site composition: class I

glutaminases possess a αβ-hydrolase fold and a catalytic Cys–His–Glu triad [14]; in contrast, class II glutaminases possess an Ntn-hydrolase fold and a catalytic N-terminal Cys. Whereas the structural basis of allosteric communication is understood to a certain degree for class II GATases [15], even a basic understanding of the allosteric communication pathways within class I GATases is still lacking.

An interesting member of class I GATases is aminodeoxychorismate synthase (ADCS), which consists of the glutaminase subunit PabA and the synthase subunit PabB. It catalyzes the committed step in the biosynthesis of folate by incorporating nitrogen into chorismate to yield 4-amino-4-deoxychorismate (Fig. 1).

Glutamine hydrolysis by PabA is activated upon complex formation with PabB and further allosterically stimulated by chorismate binding to the synthase active site. Thus, the active site of PabB acts as an *allosteric site* that, upon binding of its substrate, stimulates activity at the PabA *active site*. In spite of the identification of key catalytic amino acid residues in PabA and PabB [16,17], the availability of two PabB crystal structures [18,19], and a basic understanding of the chemical reaction mechanisms for PabA and PabB [20,21], the structural basis for allosteric communication in ADCS still awaits clarification.

Here, we addressed allostery in ADCS by a combination of experimental and computational approaches. We first solved the structure of a stable PabA subunit at high resolution. Together with the known structure of a PabB subunit, we then generated a homology model of the ADCS complex and performed a comprehensive alanine-scanning approach at conserved residues of both subunits. The results allowed us to define the allosteric communication pathway within ADCS. Specifically, we identified a conserved network of mainly hydrogen-bonded residues that propagates the signal from the *allosteric site* in PabB to the *active site* in PabA.

Results

Crystal structure analysis of PabA and homology modeling of ADCS

In order to map the allosteric communication network of ADCS, we first set out to provide the missing structural information for PabA. Despite extensive efforts, we were not able to crystallize modern PabA enzymes (from *Escherichia coli*, *Bacillus subtilis*, *Serratia marcescens*, and *Pseudomonas putida*) [22]. Ancestral sequence reconstruction often yields thermostable proteins [23], which have a higher tendency to crystallize than their thermolabile homologs. Therefore, we reconstructed ancestral PabA sequences based on the sequences of 59 recent homologs from Firmicutes, Fusobacteria, Proteobacteria, and Halobacteriales (Fig. S1). The genes encoding the three most ancient bacterial predecessors (*anc*1–3PabA) were expressed in *E. coli*, and the recombinant proteins were purified and biochemically characterized. Interestingly, all three enzymes were more thermostable than modern PabA proteins (Table S1–3), formed stable complexes with modern PabB subunits (Table S4), and were stimulated by them (Table S5). From these ancestral PabA enzymes, we were able to only crystallize *anc*2PabA and solved its structure by molecular replacement using the homologous class I glutaminase subunit from *Sulfolobus solfataricus* anthranilate synthase (AS) (PDB ID: 1QDL; sequence identity: 51%, sequence similarity: 66%) as template (Table S6). The structure of *anc*2PabA (PDB ID: 6QUR) possesses the same αβ-hydrolase fold as the glutaminase subunits of the GATases AS and imidazole glycerol phosphate synthase (ImGPS) (Fig. 2) [24–26]. The catalytic triad consisting of *a*C79, *a*H168, and *a*E170 is located at the solvent-accessible active site (*a* connotes residues in PabA, and *b* connotes residues in PabB). Surprisingly, the crystal structure of *anc*2PabA features a disulfide bond between the catalytic *a*C79 residue and *a*C54, which is located in a loop covering the active site adjacent to a sequence stretch referred to as the *oxyanion hole*

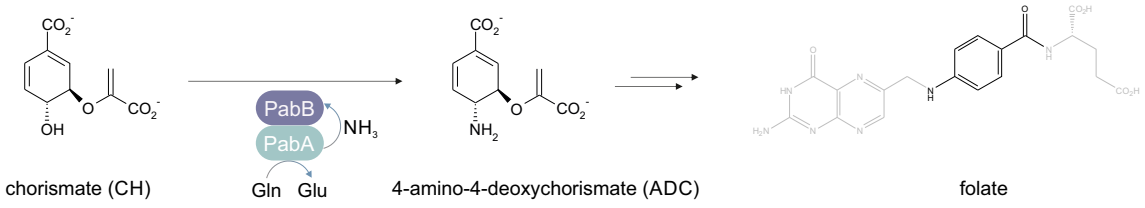

Fig. 1. Reaction catalyzed by ADCS. The glutaminase subunit PabA hydrolyzes glutamine (Gln) to glutamate (Glu) and nascent ammonia (NH_3), which is channeled to the active site of the synthase subunit PabB where it reacts with chorismate (CH) to form 4-amino-4-deoxychorismate (ADC). ADC is a precursor in the biosynthesis of folate (shown in gray except the part of the molecule that stems from ADC).

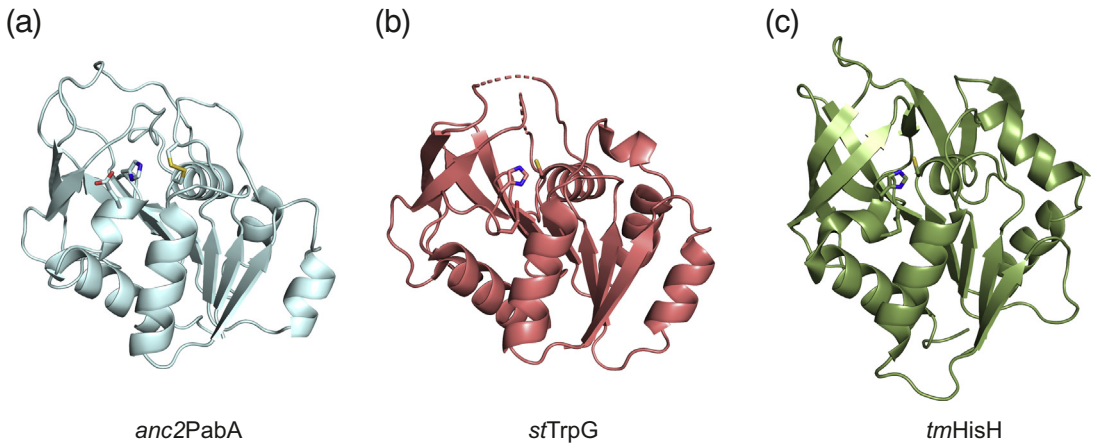

Fig. 2. Structural comparison of *anc*2PabA to homologous class I glutaminase subunits. (a) Crystal structure of *anc*2PabA (PDB ID: 6QUR); disulfide bond formed between *a*C54 and *a*C79 and the catalytic Cys–His–Glu triad is shown as sticks. (b) Crystal structure of the glutaminase subunit *st*TrpG from *Salmonella typhimurium* AS (PDB ID: 1I1Q). (c) Crystal structure of the glutaminase subunit *tm*HisH from *T. maritima* ImGPS (PDB ID: 1GPW). Sequence identity between *anc*2PabA and *st*TrpG is 84/198 (42.4%) and sequence similarity is 115/198 (58.1%). Sequence identity between *anc*2PabA and *tm*HisH is 50/231 (21.6%), and sequence similarity is 84/231 (36.4%). The structure of *anc*2PabA superimposes well with those of *st*TrpG and *tm*HisH with all-atom RMSDs of 1.6 Å (*anc*2PabA-*st*TrpG) and 2.9 Å (*anc*2PabA-*tm*HisH), respectively.

motif (*a*P51–*a*G52–*a*P53–*a*C54) [27]. Since our previous crystallization trials with a variety of modern PabA and PabA:PabB complexes failed, we assume that formation of this disulfide bond in *anc*2PabA stabilizes the enzyme and thus ultimately allowed for its crystallization.

Based on the crystal structure of *anc*2PabA, we generated a homology model for the *E. coli* ADCS complex by superimposing the previously solved *ec*PabB structure (PDB ID: 1K0E) and a model of *ec*PabA [that we generated based on the structure of *anc*2PabA (PDB ID: 6QUR)] with the homologous AS complex from *S. solfataricus* (PDB ID: 1QDL) (Table S7). To generate the final model of the holo enzyme, we superposed the substrates chorismate and glutamine from the structure of *S. marcescens* AS (PDB ID: 1I7Q) into the active sites of PabB and PabA, respectively. The model was energy minimized within YASARA's "build model" function [28] and further relaxed by molecular dynamics simulations for 100 ns with GROMACS [29,30].

Alanine scanning for the identification of residues involved in allosteric signal propagation

To identify residues in the ADCS complex that propagate the allosteric signal induced by chorismate binding to PabB onto PabA, we individually replaced 59 conserved residues located between both active sites by alanines (wild-type alanines were replaced by valines, respectively) using site-directed mutagenesis. We expressed the mutated genes in *E. coli*, purified the soluble recombinant enzymes (Table S8) and analyzed the effect of each individual mutation on complex formation and activity.

The results of analytical size exclusion chromatography showed that all mutant enzymes except those carrying the exchanges *a*Y127A, *b*D308A, and *b*R311A formed stable ADCS complexes with the corresponding wild-type partner subunit (Fig. S3 and Table S4). These three "interaction hotspot residues" are embedded in an inter-domain hydrogen bonding network that comprises residues *a*Y18, *a*Y127, *a*E170 (backbone), *a*S171, *b*D308, and *b*R311 (Fig. S2).

For the mutant enzymes that formed stable ADCS complexes with the corresponding wild-type partner subunits, we quantified the extent of allosteric PabA activation by determining the apparent glutamine hydrolysis rate (k_{app}). To this end, we incubated PabA with glutamine at saturating concentrations (20 mM) and monitored its hydrolysis before and after the addition of (i) PabB or (ii) PabB + chorismate (saturating concentrations) for all combinations of wild-type-PabA/mutant-PabB and mutant-PabA/wild-type-PabB. For the wild-type complex, the basal glutaminase activity of 0.004 s^{-1} [k_{app}(PabA)] is elevated upon binding of PabB to 0.21 s^{-1} [k_{app}(PabA + PabB)] and further allosterically stimulated in the presence of chorismate to 0.58 s^{-1} [k_{app}(PabA + PabB + CH)]. Basal glutaminase activity was similar to wild-type for all mutant enzymes, except the one containing the *a*T125A exchange (will be discussed below). In contrast, PabA activation was very sensitive to mutations in both PabA and PabB: 24 out of the 49 assayed mutant enzymes showed a more than

2-fold change in k_{app}(PabA + PabB) or k_{app}(PabA + PabB + CH) values (Table S5).

In order to identify residues that contribute to allosteric signaling, we compared the ratio of the apparent rates in the presence and absence of chorismate, which we refer to as *allosteric activation factor*. For the wild-type enzyme, the allosteric activation factor is 2.7 [0.58 s^{-1} (k_{app}(PabA + PabB + CH)]/0.21 s^{-1} (k_{app}(PabA + PabB))]. In order to exclude minor secondary effects that resulted from structural perturbations through the introduction of alanine, we defined residues as involved in allosteric signaling when their allosteric activation factor was below 1.5. Eleven mutants displayed allosteric activation factors of 1.0–1.5 indicating no or impaired allosteric activation. Thirteen mutants showed an allosteric activation factor ≤1.0, indicating allosteric deactivation (Fig. 3a).

We were interested to test whether the effects of mutations on k_{app} for glutamine hydrolysis are at least partially attributed to an increase in the Michaelis constant for glutamine (K_M^{Gln}) or entirely due to a decrease of the turnover rate (k_{cat}). For this purpose, we followed the glutamine-dependent conversion of chorismate (CH) to aminodeoxychorismate (ADC) for the different ADCS complexes (Table S9). The results demonstrated that complexes containing mutant enzymes with the exchanges *a*D6A, *a*Y8A, *a*R30A, *a*R126A, *a*H128A, *a*S129A, *a*L130A, *a*Q166A, *a*I172A *b*E119A, and *b*G207A showed drastically elevated K_M^{Gln} values, which might contribute to the observed decreases in k_{app}. The complexes containing the other mutant enzymes showed only minor effects with respect to K_M^{Gln}, proving that the observed changes in k_{app} are entirely caused by changes in k_{cat}. Interestingly, we also identified residues involved in ammonia channeling from the active site of PabA to the active site of PabB: Whereas in ADCS complexes containing mutant enzymes with the *a*D9A, *a*H101A, *a*R126A, *a*L130A, *b*D208A, *b*L309A, and *b*G369A exchanges, glutaminase activity was readily stimulated (Fig. 3a), no measurable or very low turnover was observed when the ADCS reaction was followed (Table S9). The unproductive loss of ammonia in these mutants indicates that the respective wild-type amino acids are involved in ammonia tunnel formation between active sites.

Identification of four branches of a conserved allosteric communication network

We subsequently mapped the 24 allosterically important residues on the model of *E. coli* ADCS and deduced the most plausible pathways for signal

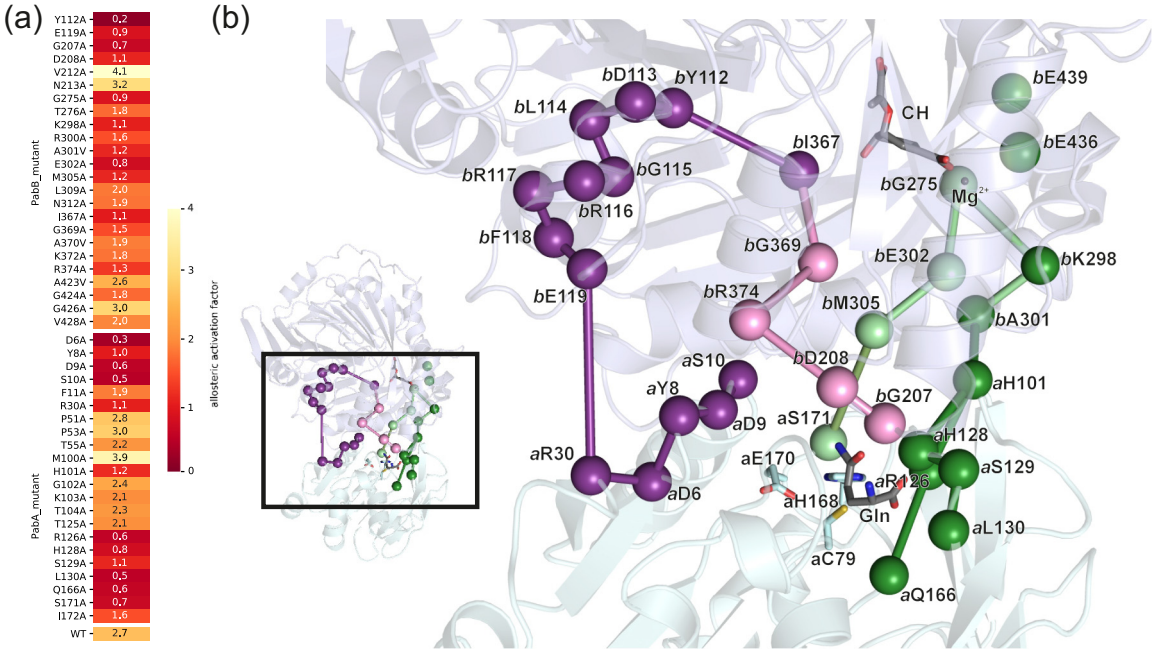

Fig. 3. Allosteric residues in ADCS. (a) Heat map indicating the ratio of the apparent glutaminase rates in the presence and absence of chorismate (k_{app}(PabA + PabB + CH)/k_{app}(PabA + PabB) = allosteric activation factor) of analyzed mutant enzymes. (b) Mapping of residues with an allosteric activation factor <1.5 on the homology model of *E. coli* ADCS (PabA is depicted in cyan, and PabB is depicted in blue). Allosterically important positions are shown as spheres (C_α), and pathways are indicated as edges connecting them. Magnesium (Mg^{2+}) in the active site of PabB is shown as sphere as well. The catalytic triad *a*C79–*a*H168–*a*E170 and the substrates glutamine and chorismate (CH) are shown as sticks. All-atom RMSD between our *E. coli* ADCS model and the crystal structure of *S. solfataricus* AS, which was used for modeling, is 1.7 Å.

propagation between the two active sites. To this end, we drew connecting edges between allosteric residues when either (i) their side chains were in direct van der Waals or hydrogen-bonding contact or (ii) the residues were connected via the protein backbone (Fig. 3b). Using this classification, we found a putative network of conserved, mostly hydrogen-bonded residues that reach from the chorismate binding site in PabB to the active site of PabA. Interestingly, this allosteric communication network appears to be split into four branches: Starting from the chorismate binding site in PabB, these branches lead to (i) the oxyanion hole motif *a*P51–*a*G52–*a*P53, to (ii) the catalytic triad *a*C79–*a*H168–*a*E170, and to (iii + iv) residues involved in glutamine binding at the PabA glutaminase active site.

The branch that leads to the oxyanion hole stretch *a*P51–*a*G52–*a*P53 supposedly senses the presence of chorismate via its hydrophobic interaction with *b*I367 located near the C4-atom of chorismate. Through a van der Waals interaction with *b*Y112, the signal might then be propagated via backbone interactions of the helix formed by residues *b*D113–*b*L114–*b*G115–*b*R116–*b*R117–*b*F118 and ultimately to *b*E119. Residue *b*E119 is located at the PabB–PabA interface and is hydrogen bonded to *a*R30. Via *a*R30, the signal is further transferred to the sequence stretch *a*Y8–*a*D9–*a*S10 adjacent to the oxyanion hole motif (Fig. 3b, purple).

The branch that leads to the catalytic triad *a*C79–*a*H168–*a*E170 presumptively senses the presence of chorismate via *b*E302, which is part of the conserved magnesium-binding site that coordinates the carboxylate group of chorismate. Via *b*E302 and the inter-domain hydrogen bonding network (Fig. S2), the signal is ultimately transferred to *a*S171, which is located adjacent to the catalytic residues *a*H168 and *a*E170 (Fig. 3b, bright green).

One branch that leads to glutamine binding residues apparently senses the presence of chorismate via *b*K298, which interacts with residues of the conserved magnesium-binding site (i.e., *b*E439 and *b*E436). The signal is then propagated via *b*A301 and *a*H101 to the glutamine binding residues *a*R126, *a*H128, *a*S129, and *a*Q166 as well as to *a*L130, which is involved in ammonia tunnel formation (Fig. 3b, dark green).

The second branch that leads to glutamine binding residues reputedly senses the presence of chorismate via *b*I367 (described above) and *b*G369 and transfers the allosteric signal via *b*R374 and *b*D208 and ultimately to *b*G207, (Fig. 3b, pink).

Analysis of a PabA mutant with increased basal glutaminase activity

Strikingly, PabA mutant *a*T125A shows a 10-fold acceleration of basal glutaminase activity [k_{app} (PabA) = 0.04 s^{-1}] compared to the wild-type enzyme [k_{app}(PabA) = 0.004 s^{-1}] (Table S5). As the allosteric activation factor (Fig. 3a) and catalytic parameters for the glutamine-dependent chorismate turnover are almost identical to wild-type ADCS (Tables S5 and S9), the wild-type *a*T125 residue seems not to be involved in the allosteric network, glutamine binding, or ammonia tunnel formation. Residue *a*T125 is hydrogen-bonded to *a*S171, an allosteric residue located adjacent to the catalytic residues *a*H168 and *a*E170 (Fig. 4a). The drastically enhanced basal glutaminase activity upon removal of this hydrogen bond in the *a*T125A mutant enzyme suggests that the relative positioning of *a*S171 with respect to the catalytic triad is crucial for glutaminase activity. We thus further analyzed the interactions of *a*S171 to other residues in ADCS. As part of the inter-domain hydrogen bonding network, *a*S171 is also hydrogen bonded to the interaction hotspot *b*D308 (Fig. S2). We generated mutant enzyme *b*D308E and monitored its ability to form stable ADCS complexes and to allosterically stimulate PabA activity. Strikingly, *b*D308E was not able to form stable ADCS complexes but led to a slightly enhanced k_{app}(PabA + PabB) and an allosteric activation factor of 1.2 (Tables S4 and S5). This finding indicates that this mutant might form a transient or weak interaction that affects the positioning of *a*S171 relative to the catalytic triad. We conclude that the corresponding wild-type residue *b*D308 undergoes a structural change in the course of signal propagation and might thus be a key residue for both complex formation and allosteric glutaminase activation within ADCS (Fig. 4b).

Discussion

Our study demonstrates that glutamine hydrolysis at the PabA subunit of ADCS is stimulated by the presence of chorismate at the PabB subunit via a conserved allosteric communication network. Starting from the chorismate binding site in PabB, the network splits into four branches that propagate the allosteric signal via mostly hydrogen-bonded residues to (i) the oxyanion hole motif *a*P51–*a*G52–*a*P53, (ii) the catalytic triad *a*C79–*a*H168–*a*E170, and (iii) glutamine binding residues at the PabA active site, respectively. In more general terms, chorismate might shift the enzyme complex from a less activated ensemble of conformational states to a more activated ensemble [31]. The deactivating effect observed in some mutants might thus result from the stabilization of the less activated ensemble by chorismate in these particular contexts.

In the following, we will discuss our findings in light of previously hypothesized activation mechanisms for different class I glutamine amidotransferase complexes. A hallmark feature of class I glutaminases is the catalytic triad composed of Cys–His–Glu, where Cys acts as nucleophile and His as general acid/base

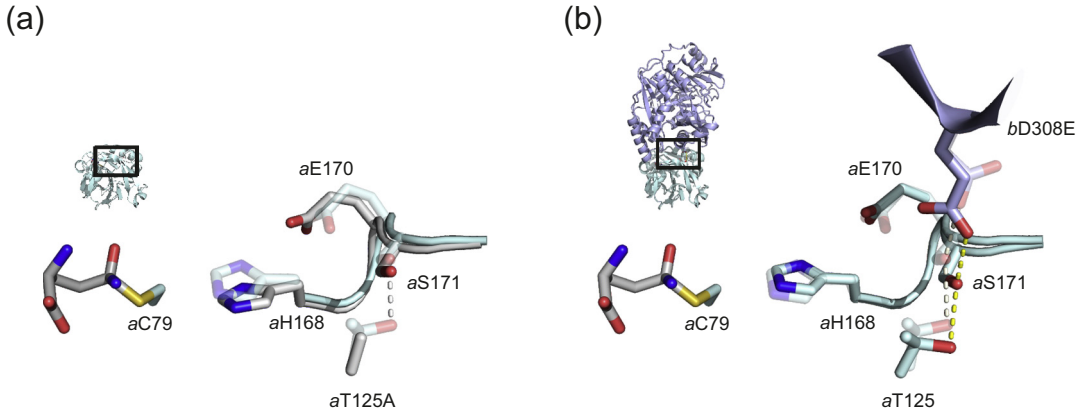

Fig. 4. Activated variants of ADCS. (a) Putative structural changes in the *a*T125A mutant enzyme: *a*T125 is hydrogen bonded to *a*S171 in wild-type PabA (transparent). The loss of the hydrogen bond toward *a*S171 in the *a*T125A mutant might allow for the movement of the loop *a*H168–*a*P169–*a*E170–*a*S171 and thereby enhance basal glutaminase activity by reducing the *a*C79–*a*H168 distance (solid). (b) Putative structural changes in the *b*D308E mutant enzyme: *b*D308 is hydrogen-bonded to *a*S171 in wild-type ADCS (transparent). A potential movement of *b*D308 in the course of allosteric signaling is mimicked through the *b*D308E mutation and might result in bending of the loop *a*H168–*a*P169–*a*E170–*a*S171 to constitutively activate the glutaminase subunit (solid).

in the catalytic cycle (Fig. 5). Glutamine hydrolysis is thereby initiated by the attack of the thiolate anion of *a*C79 (nomenclature based on *E. coli* PabA) onto the carbonyl side-chain carboxamide of glutamine to form the tetrahedral intermediate I. This intermediate is stabilized by an oxyanion hole (in ADCS formed by backbone amides of *a*G52 and *a*L80) and collapses upon protonation of the amino group by the general acid *a*H168 into ammonia and the thioester intermediate. To complete the catalytic cycle, the thioester intermediate is hydrolyzed by an activated water molecule via the tetrahedral intermediate II.

Studies on ImGPS from *Thermotoga maritima* [27,33] and pyridoxal 5′-phosphate synthase (PS) from *B. subtilis* [34] have indicated that allosteric signaling transforms the glutaminase active site from a catalysis *incompetent* to a catalysis *competent* conformation by inducing the formation of the oxyanion hole. Based on correlated motion NMR analysis and MD simulations of ImGPS, it was postulated that substrate binding to the synthase subunit HisF ultimately induces a 180° backbone flip of residue V51 in the glutaminase subunit HisH. As a result, the backbone amide of G50, which is part of the oxyanion hole, would become competent to stabilize the tetrahedral intermediates I/II. Likewise, the comparison of the crystal structures of the isolated and the associated subunits of PS has also indicated that complex formation results in a backbone flip of residue G46 in the glutaminase subunit, bringing the backbone amide of the neighbored G47 into a catalysis-competent conformation.

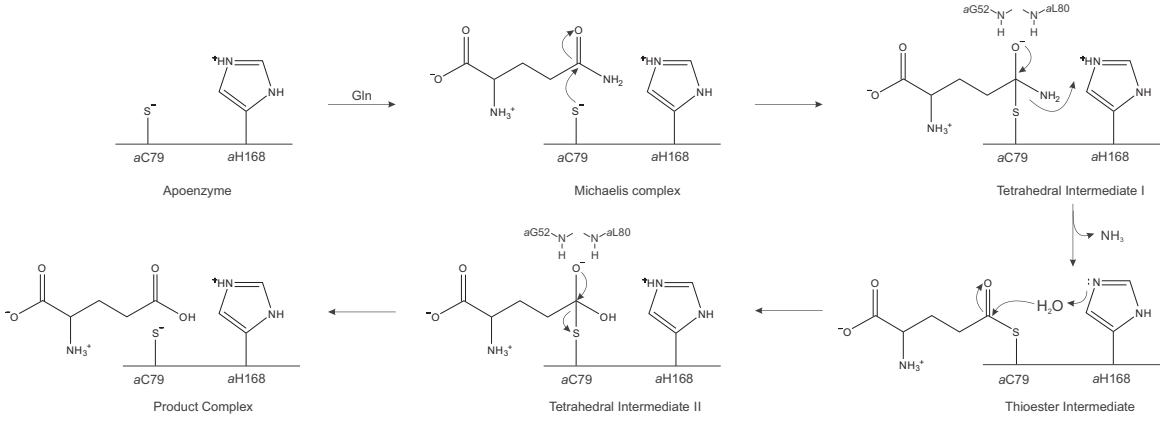

Fig. 5. Reaction mechanism of class I glutaminases. Numbering of the essential Cys and His residues has been adapted to *ec*PabA. The Glu170 residue of the catalytic triad is not shown for simplicity. The mechanism was adopted from Ref. [32].

Whereas the oxyanion hole motifs in both ImGPS (P49–G50–V51) and PS (P45–G46–G47) theoretically allow for the proposed, energetically demanding backbone flip, in ADCS the oxyanion hole motif is composed of a highly conserved *a*P51–*a*G52–*a*P53 motif, where rotation of *a*G52 around the adjacent proline residue is not possible. This indicates that more subtle reorientations lead to a catalysis-*competent* conformation in PabA. These findings for ADCS are in line with those for *Saccharomyces cerevisiae* ImGPS [35–37], *E. coli* carbamoylphosphate synthetase [32], and *E. coli* cytidine triphosphate synthetase [8] that provide no evidence for a backbone flip in their oxyanion hole motifs.

Moreover, in contrast to the postulated backbone flip in ImGPS from *T. maritima*, findings for the same enzyme from our laboratory suggested that the oxyanion hole of the glutaminase subunit HisH is in a catalysis-*competent* conformation even in the absence of substrate binding to the synthase HisF [38]. The same study showed that the mutation of HisH residues Y138 and K181 to alanines resulted in high constitutive glutaminase activity, suggesting that these amino acids are involved in the allosteric signaling pathway. Interestingly, Y138 and K181 correspond to the interaction hotspot *a*Y127 and the allosterically important residue *a*S171 identified in ADCS, respectively. Given the importance of the interaction between *a*Y127/*a*S171 and *b*D308 in ADCS, the effect of the mutations Y138A and K181A might be due to an impaired interaction with the conserved aspartate residue D98 of HisF, which corresponds to *b*D308 in ADCS. As this interaction is far apart from the oxyanion motif, it is tempting to speculate that these residues might influence the catalytic triad directly.

The analysis of two constitutively active TrpG glutaminase mutant enzymes (T129Y and T129F) of AS supports this notion, as the catalytic Cys-His distance is reduced in these mutants [39]. Interestingly, the position of T129 corresponds to *a*T125 in PabA, whose mutation to alanine also results in drastically increased basal glutamine hydrolysis. Taken together, the data obtained from the activated mutants of HisH, TrpG, and PabA indicate that a reorientation within the catalytic triad crucially contributes to glutaminase stimulation.

To conclude, our data on the allosteric communication pathway within ADCS allow us to bundle conclusions and hypotheses drawn from different laboratories on various class I GATases. Instead of attributing the allosteric activation mechanism of class I GATases exclusively to either the formation of the oxyanion hole or the reduction of distance between catalytic residues, we hypothesize an activation mechanism based on the combination of proper positioning of the oxyanion hole and glutamine-binding residues along with a distance reduction between the catalytic Cys-His residues (Fig. 6).

Materials and Methods

Cloning and mutagenesis

The genes of *ec*PabA and *ec*PabB as cloned into the pET21a expression plasmid were available from a previous study [22]. Single amino acid mutant enzymes (Table S11) were produced using a modified QuickChange mutagenesis protocol [40] with the primers listed in Table S8.

Gene expression and protein purification

Proteins were produced by gene expression in *E. coli* BL21-Gold (DE3) cells as previously described [22]. In brief, overnight cultures of individual clones were used to inoculate 1 L (*ec*PabA variants) or 2 L (*ec*PabB variants) of Luria broth medium supplemented with 150 μg/mL ampicillin. Cells were grown at 37 °C to an OD_{600} of 0.6 and then cooled to 25 °C. Expression was induced by adding 0.5 mM IPTG and growth was continued overnight at 20 °C. Cells were harvested by centrifugation (2700*g*, 4 °C), suspended in 50 mM Tris–HCl (pH 7.5), 300 mM potassium chloride, and 10 mM imidazole, and lyzed by sonification. The insoluble fraction was removed by centrifugation (23,000*g*, 4 °C), and the soluble extracts were filtered through a 0.8-μm membrane.

Supernatants containing the C-terminal hexahistidine-tagged proteins were loaded onto a HisTrapFF crude column (5 mL, GE Healthcare), which had been equilibrated with suspension buffer, and eluted from the column by applying a linear gradient of 10–750 mM imidazole. Enzyme-containing fractions, as judged by SDS-PAGE, were pooled and further purified by preparative gel filtration [Superdex 75 HiLoad 26/60, 320 mL, GE Healthcare, 50 mM Tris–HCl (pH 7.5), 50 mM KCl, 5 mM KCl, 2 mM DTT, 4 °C]. Elution fractions were analyzed by SDS-PAGE, and the fractions containing pure protein were pooled. The enzymes were finally concentrated to 50–150 μM and flash frozen in liquid nitrogen. Protein concentrations were determined by measuring the absorbance at 280 nm using the molar extinction coefficient calculated via ExPASy ProtParam (http://web.expasy.org/protparam/).

Ancestral sequence reconstruction of PabA

Methods of our standard protocol for sequence selection [41] were applied to a precompiled set of 2825 concatenated PabA and PabB sequences [22]. A subset promising a robust tree and consisting of 59 concatenated sequences from Firmicutes, Fusobacteria, Proteobacteria, and the archaeal phylum Halobacteriales were chosen for ASR. A multiple

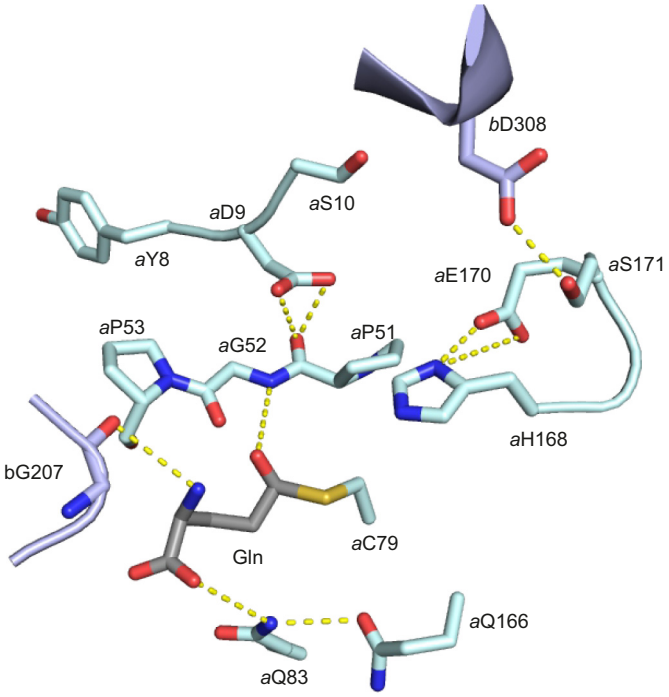

Fig. 6. Endpoints of the allosteric communication pathways in ADCS. The oxyanion hole (*a*P51–*a*G52–*a*P53) is positioned by *a*Y8, *a*D9, and *a*S10, where the substrate-induced movement of the carboxylate side chain of *a*D9 might lead to proper orientation of the oxyanion hole through interaction with the carbonyl group of *a*G52. Movement of *b*D308 toward *a*S171 might lead to a reduction of the *a*C79–*a*H168 distance by changes in the relative orientation of the *a*H168–*a*P169–*a*E170 loop. The substrate glutamine (Gln, shown as thioester intermediate) interacts via its α-amino group with the main chain carbonyl group of *b*G207, whereas its α-carboxylate group forms a hydrogen bond with the side chain of *a*Q83, which is coordinated by *a*Q166.

sequence alignment was generated by means of MAFFT [42] and solely for the computation of a phylogenetic tree that guides the subsequent reconstruction, positions containing more than 50% gaps were removed by using GBlocks [43]. The phylogenetic tree was computed with the help of pb (version 3.3 of PhyloBayes [44]) and the options -cat -gtr and by launching four independent Monte Carlo Markov Chains of length 50,000 to ensure convergence. The quality of mixing was assessed by computing for each pair of chains the discrepancy index (maxdiff, which was <0.03 in all cases) by means of bpcomp and the minimum effective size (which was >200 in all cases) with tracecomp. As all results indicated the convergence of the chains, a consensus tree was determined by means of readpb and a burn-in of 2000 (Fig. S1). The phylogeny-aware multiple sequence aligner PRANK [45] with the option -showanc was applied to the full multiple sequence alignment and the consensus tree to deduce the position of gaps in the reconstructed sequences. Their amino acid compositions were calculated with the program ancestral from PhyloBayes using midpoint rooting and the PRANK phylogeny. For the three bacterial predecessors *anc1*PabA–*anc3*PabA, which were deduced from the concatenations, the amino acid sequences are listed in Table S10.

Crystallization, data collection, and structure determination

Crystals of *anc2*PabA were obtained at 16 °C by the hanging-drop vapor diffusion method with a 500-μL reservoir consisting of 20% PEG 1500 and 40% glycerol. One microliter of a 850-μM protein solution was mixed with 1 μL of reservoir solution, and crystals grew within 10 days. Data collection was done at Swiss Light Source, Switzerland, at beamline PXIII and PXI at cryogenic temperature. The data processing was done using XDS [46,47], and the data quality assessment was done using phenix.xtriage. Molecular replacement was performed with Phaser [48] within the CCP4i [49] suite using a homology model of *anc2*PabA (generated with I-TASSER [50–52]) as template. Initial refinement was performed using REFMAC [53]. The model was further improved in several refinement rounds using automated restrained refinement with the program PHENIX [46] and interactive modeling with Coot [54]. The refinement statistics are listed in Table S6. The final model was analyzed using the program MolProbity [55].

Analysis of complex formation between different synthases and glutaminases

The ability of PabA and PabB variants to form heteromeric complexes was examined by size exclusion chromatography as previously described [22]. In brief, the experimental setup of SEC comprised Superdex 75 10/300 GL column (GE Healthcare) operated on an ÄKTAmicro system (GE Healthcare) connected to an ALIAS autosampler (Spark Holland). The system was operated at 25 °C with a flow rate of 0.5 mL/min of degassed buffer [50 mM Tris–HCl (pH 7.5), 150 mM KCl, 5 mM $MgCl_2$] and was calibrated with conalbumin, ovalbumin, carbonic anhydrase, ribonuclease A, and aprotinin from the GE Healthcare SEC Low-Molecular-Weight as well as the SEC High-Molecular-Weight calibration kit.

Individual synthases and glutaminases were assayed at a concentration of 50 μM (applied volume 50 μL). For analysis of complex formation, synthases and glutaminases were equimolarly mixed to a final concentration of 50 μM.

Steady-state enzyme kinetics

The glutaminase activity was measured spectrophotometrically in a coupled enzymatic assay as previously described [22]. In brief, glutamate formed by the glutaminase was converted to α-ketoglutarate by glutamate-dehydrogenase with simultaneous reduction of NAD^+ to NADH. A standard assay contained 50 mM Tricine–KOH buffer (pH 8.0), 5 mM $MgCl_2$, 1 mM DTT, 10 mM NAD^+, 1 mg/mL glutamate-dehydrogenase, and 20 mM glutamine. Following preincubation, 1 μM glutaminase PabA was added, and the reaction was monitored at 340 nm and 25 °C for 20 min. After making sure that the progress curve proceeded with a constant slope, 3 μM synthase PabB or 3 μM synthase PabB +200 μM chorismate were added and the reaction was again monitored for at least 10 min. The slopes of the linear parts of the progress curves before and after the addition of the synthase/synthase + chorismate were used to calculate the apparent turnover rate upon the addition of the synthase/synthase + chorismate. The ratio of the apparent turnover rates in the presence and absence of chorismate was used to calculate allosteric activation factors. Slopes were determined and calculations performed within a custom Python script.

The PabB reaction was measured at 25 °C using an assay monitoring para-aminobenzoic acid fluorescence (excitation 320 nm, emission 350 nm) [22]. For this purpose, the PabB product 4-amino-4-deoxychorismate was converted *in situ* to para-aminobenzoic acid by a molar excess of 4-amino-4-deoxychorismate lyase (PabC). A standard glutamine-depending assay contained 100 mM potassium phosphate buffer (pH 7.0), 5 mM $MgCl_2$, 1 mM DTT, 10 μM PabC, 200 μM CH, and 1.5 μM PabB and 0.5 μM PabA. After preincubation, 0–10 mM glutamine was added. For each individual substrate concentration, progress curves were collected and fitted to the Michaelis–Menten equation in a custom Python script to derive k_{cat} and K_M^{Gln}.

Thermal stability of purified proteins

Melting temperatures of purified proteins were determined with nano-differential scanning fluorimetry in a Prometheus NT.48 (NanoTemper, Munich) at the facilities of 2bind molecular interactions in Regensburg. Typically, 10 μL of a 100-μM protein solution was loaded into glass capillaries, and intrinsic tryptophan fluorescence emission intensities $F_{330\ nm}$ and $F_{350\ nm}$ were measured from 20 to 95 °C. The maxima of first derivatives of $F_{330\ nm}/F_{350\ nm}$ were used to derive the melting temperature T_M at which half of the protein is denatured.

Accession numbers

*ec*PabA_WT—NCBI Reference Sequence: WP_115194528.
*ec*PabB_W—NCBI Reference Sequence: WP_000854958.
*anc*2PabA—PDB ID: 6QUR

CRediT authorship contribution statement

Florian Semmelmann: Conceptualization, Writing - original draft. **Kristina Straub:** Investigation, Writing - original draft. **Julian Nazet:** Investigation. **Chitra Rajendran:** Investigation, Writing - original draft. **Rainer Merkl:** Conceptualization, Supervision, Writing - review & editing. **Reinhard Sterner:** Conceptualization, Supervision, Writing - review & editing.

Acknowledgments

F.S. was supported by a doctoral fellowship from the Konrad-Adenauer-Stiftung. We thank Christiane Endres, Sonja Fuchs, Sabine Laberer, Ulrike Stöckl, and Jeannette Ueckert for expert technical assistance. We thank 2bind molecular interactions GmbH for access to Prometheus NT.48 and consumables.

Author Contributions: Conceptualization: F.S., R.M., R.S. - Investigation: F.S., K.S., J.N., C.R. - Supervision: R.M., R.S. - Writing: - original draft: F. S., K.S., C.R. - Writing - review & editing: R.M., R.S.

Declaration of Competing Interest: The authors declare that they have no competing financial interests.

Appendix A. Supplementary data

Supplementary data to this article can be found online at https://doi.org/10.1016/j.jmb.2019.05.021.

Received 4 March 2019;
Received in revised form 10 May 2019;
Available online 21 May 2019

Keywords:
allostery;
ancestral sequence reconstruction;
bi-enzyme complex;
catalytic triad;
glutamine amidotransferases

Abbreviations used:
GATases, glutamine amidotransferases; ADCS,

aminodeoxychorismate synthase; AS, anthranilate synthase; ImGPS, imidazole glycerol phosphate synthase.

References

[1] J. Monod, J. Wyman, J.-P. Changeux, On the nature of allosteric transitions: a plausible model, J. Mol. Biol. 12 (1965) 228-113.

[2] Y.-N.P. Chen, M.J. LaMarche, H.M. Chan, P. Fekkes, J. Garcia-Fortanet, M.G. Acker, et al., Allosteric inhibition of shp2 phosphatase inhibits cancers driven by receptor tyrosine kinases, Nature 535 (2016) 148–152.

[3] D.T. Monaghan, M.W. Irvine, B.M. Costa, G. Fang, D.E. Jane, Pharmacological modulation of nmda receptor activity and the advent of negative and positive allosteric modulators, Neurochem. Int. 61 (2012) 581–592.

[4] Z. Fang, C. Grütter, D. Rauh, Strategies for the selective regulation of kinases with allosteric modulators: exploiting exclusive structural features, ACS Chem. Biol. 8 (2012) 58–70.

[5] P.E. Selvy, R.R. Lavieri, C.W. Lindsley, H.A. Brown, Phospholipase d: enzymology, functionality, and chemical modulation, Chem. Rev. 111 (2011) 6064–6119.

[6] T. Kenakin, L.J. Miller, Seven transmembrane receptors as shapeshifting proteins: the impact of allosteric modulation and functional selectivity on new drug discovery, Pharmacol. Rev. 62 (2010) 265–304.

[7] I. Rivalta, G.P. Lisi, N.-S. Snoeberger, G. Manley, J.P. Loria, V.S. Batista, Allosteric communication disrupted by a small molecule binding to the imidazole glycerol phosphate synthase protein–protein interface, Biochemistry 55 (2016) 6484–6494.

[8] M. Goto, R. Omi, N. Nakagawa, I. Miyahara, K. Hirotsu, Crystal structures of CTP synthetase reveal ATP, UTP, and glutamine binding sites, Structure 12 (2004) 1413–1423.

[9] K. Gunasekaran, B. Ma, R. Nussinov, Is allostery an intrinsic property of all dynamic proteins? Proteins: Struct., Funct., Bioinf. 57 (2004) 433–443.

[10] S. Mouilleron, B. Golinelli-Pimpaneau, Conformational changes in ammonia-channeling glutamine amidotransferases, Curr. Opin. Struct. Biol. 17 (2007) 653–664.

[11] F.M. Raushel, J.B. Thoden, H.M. Holden, The amidotransferase family of enzymes: molecular machines for the production and delivery of ammonia, Biochemistry 38 (1999) 7891–7899.

[12] H. Zalkin, J.L. Smith, Enzymes utilizing glutamine as an amide donor, Adv. Enzymol. Relat. Areas Mol. Biol. 72 (1998) 87–144.

[13] J.A. Brannigan, G. Dodson, H.J. Duggleby, P.C. Moody, J.L. Smith, D.R. Tomchick, et al., A protein catalytic framework with an N-terminal nucleophile is capable of self-activation, Nature 378 (1995) 416–419.

[14] D.L. Ollis, E. Cheah, M. Cygler, B. Dijkstra, F. Frolow, S.M. Franken, et al., The α/β hydrolase fold, Protein Eng. 5 (1992) 197–211.

[15] S. Mouilleron, M.A. Badet-Denisot, B. Badet, B. Golinelli-Pimpaneau, Dynamics of glucosamine-6-phosphate synthase catalysis, Arch. Biochem. Biophys. 505 (2011) 1–12.

[16] E.A. Rayl, J.M. Green, B.P. Nichols, *Escherichia coli* aminodeoxychorismate synthase: analysis of PabB mutations affecting catalysis and subunit association, Biochim. Biophys. Acta Protein Struct. Mol. Enzymol. 1295 (1996) 81–88.

[17] B. Roux, C.T. Walsh, P-aminobenzoate synthesis in *Escherichia coli*: kinetic and mechanistic characterization of the amidotransferase PabA, Biochemistry 31 (1992) 6904–6910.

[18] J.F. Parsons, P.Y. Jensen, A.S. Pachikara, A.J. Howard, E. Eisenstein, J.E. Ladner, Structure of *Escherichia coli* aminodeoxychorismate synthase: architectural conservation and diversity in chorismate-utilizing enzymes, Biochemistry 41 (2002) 2198–2208.

[19] A.K. Bera, V. Atanasova, A. Dhanda, J.E. Ladner, J.F. Parsons, Structure of aminodeoxychorismate synthase from *Stenotrophomonas maltophilia*, Biochemistry 51 (2012) 10208–10217.

[20] Z. He, K.D. Stigers Lavoie, P.A. Bartlett, M.D. Toney, Conservation of mechanism in three chorismate-utilizing enzymes, J. Am. Chem. Soc. 126 (2004) 2378–2385.

[21] J.E. Culbertson, D.h. Chung, K.T. Ziebart, E. Espiritu, M.D. Toney, Conversion of aminodeoxychorismate synthase into anthranilate synthase with janus mutations: mechanism of pyruvate elimination catalyzed by chorismate enzymes, Biochemistry 54 (2015) 2372–2384.

[22] M.G. Plach, F. Semmelmann, F. Busch, M. Busch, L. Heizinger, V.H. Wysocki, et al., Evolutionary diversification of protein–protein interactions by interface add-ons, Proc. Natl. Acad. Sci. U. S. A. 114 (2017) E8333–E8342.

[23] L.C. Wheeler, S.A. Lim, S. Marqusee, M.J. Harms, The thermostability and specificity of ancient proteins, Curr. Opin. Struct. Biol. 38 (2016) 37–43.

[24] A.A. Morollo, M.J. Eck, Structure of the cooperative allosteric anthranilate synthase from *Salmonella typhimurium*, Nat. Struct. Mol. Biol. 8 (2001) 243.

[25] T. Knöchel, A. Ivens, G. Hester, A. Gonzalez, R. Bauerle, M. Wilmanns, et al., The crystal structure of anthranilate synthase from *Sulfolobus solfataricus*: functional implications, Proc. Natl. Acad. Sci. 96 (1999) 9479–9484.

[26] A. Douangamath, M. Walker, S. Beismann-Driemeyer, M.C. Vega-Fernandez, R. Sterner, M. Wilmanns, Structural evidence for ammonia tunneling across the $(\beta\alpha)_8$- barrel of the imidazole glycerol phosphate synthase bienzyme complex, Structure 10 (2002) 185–193.

[27] I. Rivalta, M.M. Sultan, N.-S. Lee, G.A. Manley, J.P. Loria, V. S. Batista, Allosteric pathways in imidazole glycerol phosphate synthase, Proc. Natl. Acad. Sci. U. S. A. 109 (2012) E1428–E1436.

[28] E. Krieger, G. Vriend, Yasara view—molecular graphics for all devices—from smartphones to workstations, Bioinformatics 30 (2014) 2981–2982.

[29] H.J. Berendsen, D. van der Spoel, R. van Drunen, Gromacs: a message-passing parallel molecular dynamics implementation, Comput. Phys. Commun. 91 (1995) 43–56.

[30] E. Lindahl, B. Hess, D. Van Der Spoel, Gromacs 3.0: a package for molecular simulation and trajectory analysis, Mol. Model. Ann. 7 (2001) 306–317.

[31] H.N. Motlagh, J.O. Wrabl, J. Li, V.J. Hilser, The ensemble nature of allostery, Nature 508 (2014) 331–339.

[32] J.B. Thoden, X. Huang, F.M. Raushel, H.M. Holden, The small subunit of carbamoyl phosphate synthetase: snapshots along the reaction pathway, Biochemistry 38 (1999) 16158–16166.

[33] J.M. Lipchock, J.P. Loria, Nanometer propagation of millisecond motions in v-type allostery, Structure 18 (2010) 1596–1607.

[34] M. Strohmeier, T. Raschle, J. Mazurkiewicz, K. Rippe, I. Sinning, T.B. Fitzpatrick, et al., Structure of a bacterial

pyridoxal 5′-phosphate synthase complex, Proc. Natl. Acad. Sci. 103 (2006) 19284–19289.
[35] B.N. Chaudhuri, S.C. Lange, R.S. Myers, V.J. Davisson, J.L. Smith, Toward understanding the mechanism of the complex cyclization reaction catalyzed by imidazole glycerolphosphate synthase: crystal structures of a ternary complex and the free enzyme, Biochemistry 42 (2003) 7003–7012.
[36] R.S. Myers, R.E. Amaro, Z.A. Luthey-Schulten, V.J. Davisson, Reaction coupling through interdomain contacts in imidazole glycerol phosphate synthase, Biochemistry 44 (2005) 11974–11985.
[37] R.E. Amaro, A. Sethi, R.S. Myers, V.J. Davisson, Z.A. Luthey-Schulten, A network of conserved interactions regulates the allosteric signal in a glutamine amidotransferase, Biochemistry 46 (2007) 2156–2173.
[38] F. List, M.C. Vega, A. Razeto, M.C. Häger, R. Sterner, M. Wilmanns, Catalysis uncoupling in a glutamine amidotransferase bienzyme by unblocking the glutaminase active site, Chem. Biol. 19 (2012) 1589–1599.
[39] F. List, M. Bocola, M.C. Häger, R. Sterner, Constitutively active glutaminase variants provide insights into the activation mechanism of anthranilate synthase, Biochemistry 51 (2012) 2812–2818.
[40] W. Wang, B.A. Malcolm, Two-stage PCR protocol allowing introduction of multiple mutations, deletions and insertions using QuikChange site-directed mutagenesis, BioTechniques 26 (1999) 680–682.
[41] K. Straub, R. Merkl, Ancestral sequence reconstruction as a tool for the elucidation of a stepwise evolutionary adaptation, in: T. Sikosek (Ed.), Computational Methods in Protein Evolution, Humana Press, New York, NY 2019, pp. 171–182.
[42] K. Katoh, D.M. Standley, Mafft multiple sequence alignment software version 7: improvements in performance and usability, Mol. Biol. Evol. 30 (2013) 772–780.
[43] J. Castresana, Selection of conserved blocks from multiple alignments for their use in phylogenetic analysis, Mol. Biol. Evol. 17 (2000) 540–552.
[44] N. Lartillot, T. Lepage, S. Blanquart, Phylobayes 3: a Bayesian software package for phylogenetic reconstruction and molecular dating, Bioinformatics 25 (2009) 2286–2288.
[45] A. Löytynoja, N. Goldman, Phylogeny-aware gap placement prevents errors in sequence alignment and evolutionary analysis, Science 320 (2008) 1632–1635.
[46] P.D. Adams, R.W. Grosse-Kunstleve, L.-W. Hung, T.R. Ioerger, A.J. McCoy, N.W. Moriarty, et al., Phenix: building new software for automated crystallographic structure determination, Acta Crystallogr. D Biol. Crystallogr. 58 (2002) 1948–1954.
[47] W. Kabsch, Automatic processing of rotation diffraction data from crystals of initially unknown symmetry and cell constants, J. Appl. Crystallogr. 26 (1993) 795–800.
[48] A.J. McCoy, R.W. Grosse-Kunstleve, P.D. Adams, M.D. Winn, L.C. Storoni, R.J. Read, Phaser crystallographic software, J. Appl. Crystallogr. 40 (2007) 658–674.
[49] L. Potterton, S. McNicholas, E. Krissinel, J. Gruber, K. Cowtan, P. Emsley, et al., Developments in the ccp4 molecular-graphics project, Acta Crystallogr. sect. D: Biol. Crystallogr. 60 (2004) 2288–2294.
[50] Y. Zhang, I-TASSER server for protein 3d structure prediction, BMC Bioinf. 9 (2008) 40.
[51] A. Roy, A. Kucukural, Y. Zhang, I-TASSER: a unified platform for automated protein structure and function prediction, Nat. Protoc. 5 (2010) 725.
[52] J. Yang, R. Yan, A. Roy, D. Xu, J. Poisson, Y. Zhang, The I-TASSER suite: protein structure and function prediction, Nat. Methods 12 (2015) 7.
[53] G.N. Murshudov, A.A. Vagin, E.J. Dodson, Refinement of macromolecular structures by the maximum-likelihood method, Acta Crystallogr. Sect. D 53 (1997) 240–255.
[54] P. Emsley, K. Cowtan, Coot: model-building tools for molecular graphics, Acta Crystallogr. D Biol. Crystallogr. 60 (2004) 2126–2132.
[55] I.W. Davis, A. Leaver-Fay, V.B. Chen, J.N. Block, G.J. Kapral, X. Wang, et al., Molprobity: all-atom contacts and structure validation for proteins and nucleic acids, Nucleic Acids Res. 35 (2007) W375–W383.